# Chapter 9
# Quantitative fMRI

**N. P. Blockley, V. E. M. Griffeth, A. B. Simon and R. B. Buxton**

## Introduction

Since its discovery in 1990, blood oxygenation level-dependent (BOLD) MRI has proven in countless studies to be a powerful and sensitive tool for noninvasively detecting neural activity changes in the brain (Ogawa et al. 1990), with superior spatial resolution to EEG, magnetoencephalography (MEG), and positron emission tomography (PET). The complex and incompletely understood physiologic phenomenon underlying the BOLD response is a neurovascular signaling process that increases blood flow to regions of increased neural and metabolic activity disproportionately to the smaller change in oxygen metabolism (Fox and Raichle 1986). As a result, the local venous blood is more oxygenated when neural activity increases, and the magnetic resonance (MR) signal is uniquely sensitive to the oxygenation of blood. This sensitivity is determined by the oxygenation state of the hemoglobin contained within the red blood cells, or, more accurately, the proportion of hemoglobin that is deoxygenated (Thulborn et al. 1982). The paramagnetic nature of deoxyhemoglobin causes the transverse relaxation time, $T_2^*$, to increase as the concentration of deoxyhemoglobin reduces, so that the MR signal increases with neural activation.

N. P. Blockley (✉) · R. B. Buxton
Department of Radiology, Center for Functional MRI, University of California San Diego, 9500 Gilman Drive, MC 0677, La Jolla, CA 92093-0677, USA
e-mail: nicholas.blockley@ndcn.ox.ac.uk

FMRIB Centre, Nuffield Department of Clinical Neurosciences, University of Oxford, John Radcliffe Hospital, Headington, Oxford, OX3 9DU, UK

V. E. M. Griffeth · A. B. Simon
Department of Bioengineering and Medical Scientist Training Program, University of California San Diego, 9500 Gilman Drive, La Jolla, CA 92093, USA

R. B. Buxton
Kavli Institute for Brain and Mind, University of California San Diego, 9500 Gilman Drive, La Jolla, CA 92093, USA



K. Uludağ et al. (eds.), *fMRI: From Nuclear Spins to Brain Functions,*
Biological Magnetic Resonance 30, DOI 10.1007/978-1-4899-7591-1_9

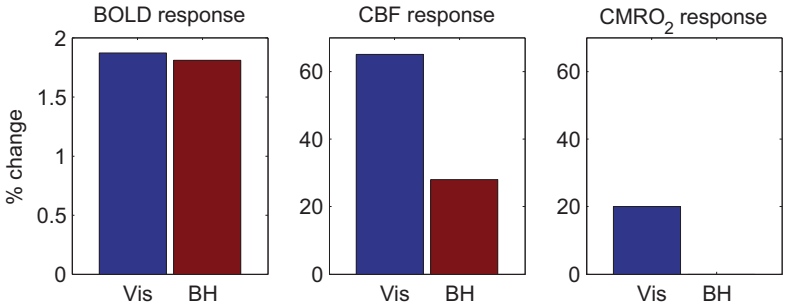


**Fig. 9.1** The measured BOLD response to a visual stimulus *(Vis)* and a breath hold *(BH)* reveals differences in the underlying CBF and $CMRO_2$ responses. The BOLD responses are similar, suggesting similar changes in the deoxyhemoglobin content of tissue. Yet the CBF response is much larger to the visual stimulus because the CBF effect on blood oxygenation is partly offset by the $CMRO_2$ change, while the breath hold is purely dependent on CBF

However, the complex decoupling of local blood flow and oxygen metabolism that provides BOLD imaging with its endogenous contrast proves to be a problem when it comes to comparing BOLD responses quantitatively across subjects, imaging sites, and time. The difficulty in quantifying the BOLD response lies in the fact that BOLD imaging is not directly sensitive to cerebral metabolic activity, but rather to the amount of deoxygenated hemoglobin in the capillaries and venules of brain tissue (Ogawa et al. 1993). This quantity, in turn, depends upon the oxygen saturation of arterial blood, the hematocrit, and changes in the volume of blood in the cerebral tissue (cerebral blood volume—CBV), the local rate of oxygen metabolism (cerebral metabolic rate of $O_2$ metabolism—$CMRO_2$), and the rate at which oxygen-rich blood is delivered to the tissue (cerebral blood flow—CBF). Due to this complexity, it is possible to generate similar BOLD responses with very different underlying changes in CBF, CBV, and $CMRO_2$.

To illustrate this, let us consider a simple experiment in which the subject is exposed to two different stimuli. First, the subject is asked to watch a flickering checkerboard, which is widely used to activate the primary visual cortex (V1) of the brain. As Fig. 9.1 illustrates, neural activity in the visual cortex increases the local $CMRO_2$ as well as the blood flow to V1. Because the blood flow increases disproportionately to $CMRO_2$ (Fox and Raichle 1986), the oxygen saturation of blood in the capillaries and veins increases in the activated region. The second stimulus requires the subject to hold their breath for a similar period of time as the visual stimulus. This causes the arterial blood carbon dioxide concentration to increase, which has a vasodilatory effect on cerebral arterioles causing blood flow to increase across the brain. Now, rather than eliciting neural activity with a sensory stimulus, the experimenter is causing blood flow to increase without changing the metabolic rate (Davis et al. 1998). Imaging V1 using BOLD functional magnetic resonance imaging (fMRI) will produce detectible increases in BOLD signal for both stimuli, yet only one of these stimuli has provoked significant neural activity. As Fig. 9.1 shows, the BOLD signal changes in response to both stimuli are very similar, although the underlying changes in CBF and $CMRO_2$ are not. As the effects of $CMRO_2$ and

CBF cause opposing changes in the BOLD signal, CBF must increase to a greater degree in response to a visual stimulus to give a comparable BOLD response. Since the BOLD response to a breath hold is entirely determined by changes in CBF, this change need not be as large.

This simple example demonstrates that without further physiological measurements, it is not possible to be certain which components of the measured BOLD response are due to metabolic or vascular responses. A tool with which to quantify the BOLD signal in terms of oxidative metabolism would have applications beyond improving the accuracy of functional mapping. For example, during pharmacological manipulations, it is important to be able to separate the vascular and neural effects of psychoactive drugs. Experiments with acetazolamide have helped to illustrate this point (Brown et al. 2003). Acetazolamide has cerebrovascular effects that are similar to those observed during hypercapnia whereby blood flow is increased. It is also known to have very little effect on $CMRO_2$ or the underlying neural activity (Vorstrup et al. 1984). Brown et al. observed that the BOLD response to a motor task was decreased following administration of acetazolamide. Without blood flow data, which were simultaneously acquired, it would have been difficult to determine whether this change was neural or vascular in origin. Blood flow data revealed that although the global baseline CBF was increased, the absolute change in response to the stimulus was unchanged between the normal and pharmacological states. This underlines the influence of the baseline physiology on the magnitude of the BOLD response. The baseline state is also important for interpreting BOLD studies in disease, where both the response to a stimulus and the baseline state may be altered, either due to the disease itself or due to medications. For example, a recent study of subjects at risk for Alzheimer's disease not only found decreased BOLD responses to a memory task but also an elevated resting CBF in the medial temporal lobes, suggesting that the change in the acute BOLD response to the task may in fact reflect a more chronic aspect of the disease (Fleisher et al. 2009). Therefore, without measurement of CBF, the analysis of functional BOLD responses is seriously confounded. A further example can be drawn from a recent study of attention. When a subject voluntarily attended to a visual stimulus, the blood flow response increased much more than the BOLD response, consistent with attention, creating a stronger modulation of the $CMRO_2$ response (Moradi and Buxton 2011).

Attempts to quantify the BOLD response in terms of $CMRO_2$ generally rely on additional measurements of at least one of the underlying components of the signal. Typically, this is through measurements of CBF (Davis et al. 1998; Hoge et al. 1999; Kim et al. 1999), but this is sometimes supplemented with a measure of CBV (Lin et al. 2008). These MRI techniques are already quantitative measurements of physiological processes; however, in the context of this chapter, their use shall be considered in support of a better understanding of the BOLD response. In combination with the BOLD effect, these techniques offer the prospect of measuring $CMRO_2$, which is directly linked to the energy costs of neural activity rather than to a secondary vascular effect. The focus of this chapter is to consider how $CMRO_2$ may be measured along with how it affects the BOLD signal. Currently, the most widely used method for quantifying $CMRO_2$ changes with functional activation is the calibrated BOLD method introduced by Davis et al. (1998). This approach

typically uses an arterial spin-labeling (ASL) method to measure the CBF response as well as the BOLD response to activation, and is based on the idea that the BOLD response magnitude depends on both the CBF and $CMRO_2$ responses. With a separate measurement of the CBF response, the $CMRO_2$ response can be estimated. In addition, two promising approaches for quantifying baseline $CMRO_2$ ($T_2$ relaxation under spin tagging—TRUST and quantitative BOLD—qBOLD) are also based on the relaxation time changes created by changes in deoxyhemoglobin concentration. The TRUST method enables whole-head measurements of $CMRO_2$ in the steady state, giving useful information about the baseline physiological state (Lu and Ge 2008). However, the whole-head nature of this technique limits it to stimuli with global effects. The qBOLD technique is similarly limited to steady-state, or slowly changing measurements of $CMRO_2$ (An and Lin 2000; He and Yablonskiy 2007). This technique enables absolute $CMRO_2$ to be calculated at the tissue level, but relies on detailed modeling hampering its widespread utilization so far. This chapter presents a review of these methods, including the underlying principles, methodology, and limitations.

## Understanding the BOLD Response

### *The Problem of Interpreting the BOLD Response in a Quantitative Way*

As stated in the introduction, interpreting relative intensities of BOLD activation in terms of neural activity is more difficult than mapping where the activation occurred due to the complex dependence of the BOLD signal on CBF, CBV, and $CMRO_2$ (Fig. 9.2). This complex dependence is a direct consequence of the source of the BOLD signal, deoxyhemoglobin, which is paramagnetic, while oxyhemoglobin is not (Pauling and Coryell 1936). The amount of deoxyhemoglobin present determines the magnetic susceptibility of blood and alters the magnetic resonance

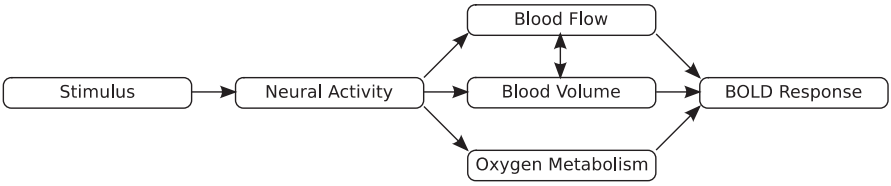


**Fig. 9.2** The BOLD response is driven by neural activity through parallel changes in blood flow/volume and oxidative metabolism. The complexity of interpretation of BOLD signals arises because increased blood flow and oxygen metabolism drive the BOLD response in opposite directions. The quantitative picture is even more complicated because increased venous blood volume tends to decrease the BOLD response, while increased arterial blood volume may increase the measured BOLD response through a volume exchange effect

(MR) signal, both within the vessel and surrounding it (Ogawa et al. 1990). Arterial blood is delivered to tissue fully oxygenated and, at rest, about 40 % of the oxygen is extracted as blood passes through the capillary bed, creating a significant amount of deoxyhemoglobin in the venous and capillary vasculature (Marchal et al. 1992). Only small changes in the MR signal would be detected if the oxygen extraction fraction (OEF) and deoxyhemoglobin concentrations remain constant during activation, resulting from a volume exchange effect (Uludağ et al. 2009). However, with neural activation, increases in CBF are much greater than increases in $CMRO_2$ (Fox and Raichle 1986), leading to a decrease in the OEF and a reduction in the concentration of deoxyhemoglobin. This uncoupling of CBF and $CMRO_2$ causes a disproportionate increase in blood oxygenation during neural activation and is the root of the BOLD response. Variations in CBV add to this complexity by altering the total amount of blood containing deoxyhemoglobin and through a volume exchange effect, whereby intravascular volume replaces extravascular volume upon activation.

Establishing a firm understanding of the relationship between the BOLD signal and the underlying neurophysiology, including CBF, CBV, and $CMRO_2$, remains a challenging yet essential task for accurate interpretation of fMRI studies. With activation, all three of these physiologic variables increase, but they have conflicting effects on the local deoxyhemoglobin concentration and thus the BOLD response. The CBF change tends to wash out local deoxyhemoglobin and increase the BOLD response, while the $CMRO_2$ change tends to increase deoxyhemoglobin and decrease the BOLD response. The effect of CBV provides an additional complication. An increase of venous CBV will increase local deoxyhemoglobin and tend to decrease the BOLD response. At first glance, an increase of arterial CBV would seem to have no effect on the BOLD response, because there is little deoxyhemoglobin in the arterial vessels and hence a limited extravascular effect. However, an increase in blood volume may cause a redistribution of the other components of the voxel, that is, movement of cerebrospinal fluid (CSF). This can cause an additional signal contribution to the measured BOLD response due to this exchange of volumes if the intrinsic signals differ. This effect is not "blood oxygenation dependent," but is nevertheless present in the measured BOLD signal. At typical clinical field strengths of 1.5–3.0 T, the intrinsic signal of arterial blood is higher than the tissue, so arterial CBV changes may increase the BOLD response. This is not the case at higher field strengths where the arterial blood relaxation rate is greater than that of the tissue leading to a reduction in MR signal (Uludağ 2010).

The concentration of deoxyhemoglobin thus is determined by CBF, CBV, and $CMRO_2$, where the conversion of oxyhemoglobin into deoxyhemoglobin reflects $CMRO_2$. Blood flow acts to replenish the vasculature with oxyhemoglobin and wash out deoxyhemoglobin, while CBV acts as a reservoir for containment. At steady state, this relationship can be described for the venous compartment by using Fick's principle. This principle describes the conservation of oxygen delivered and consumed, whereby that delivered is proportional to CBF and the arteriovenous oxygen difference (Guyton 1991). Since the arteriovenous oxygen difference is proportional to deoxyhemoglobin production, the venous deoxyhemoglobin concentration, [dHb], can be written in terms of $CMRO_2$ and CBF.

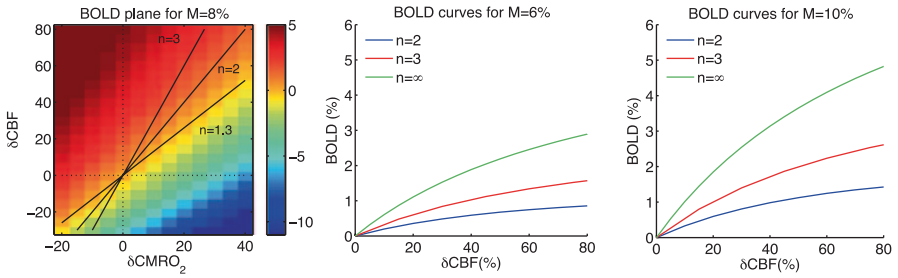


**Fig. 9.3** The BOLD response is driven by the CBF response, but strongly modulated by two other physiological parameters: the ratio of the fractional CBF change to the fractional $CMRO_2$ change *(n)* and the deoxyhemoglobin content in the baseline state expressed as a scaling factor *M*. The BOLD plane *(left panel)* shows how the BOLD response (color coded as a percent signal change) is affected by CBF and $CMRO_2$ changes (also as percent changes from baseline). Plots of BOLD versus CBF *(middle* and *right panels)* illustrate the modulating effects of different values of *M* and *n*: For the same underlying change in CBF, the BOLD response increases for larger *M* or *n*. Calculations assumed the Davis model

$$[\,\mathrm{dHb}\,] \propto \frac{\mathrm{CMRO_2}}{\mathrm{CBF}} \tag{9.1}$$

The total amount of deoxyhemoglobin present in the voxel is then determined by CBV.

While we generally think of the BOLD response as being driven by the change in CBF, there are two confounding effects that strongly modulate the BOLD signal, even for the same underlying change in neural activity. These are the baseline level of deoxyhemoglobin and the coupling of CBF and $CMRO_2$ changes. Figure 9.3a plots the BOLD signal plane for a continuum of CBF and $CMRO_2$ changes for a single baseline level. The baseline amount of deoxyhemoglobin sets the dynamic range of the BOLD response. Since increases in BOLD signal are caused by a reduction in the deoxyhemoglobin content of venous blood, the signal cannot increase beyond the point that this blood is fully oxygenated (OEF = 0). This is known as the "ceiling effect" (Buxton 2010) and is an important confounding factor when studying populations affected by drugs (Brown et al. 2003; Uludağ and Buxton 2004; Perthen et al. 2008), disease (Fleisher et al. 2009), or even aging (Ances et al. 2009), where the baseline CBF and $CMRO_2$ may be altered. Figure 9.3b, c shows the effect of different baseline physiological levels on the BOLD signal. Each baseline level is described by a constant, *M*, and reveals that only small changes are required to produce large alterations in BOLD signal. In addition to variation within a subject or patient population, regional (Lammertsma 1984; Derdeyn et al. 2002) and temporal (Bremmer et al. 2010) variation in baseline CBV and OEF may create further disparity in the baseline level of deoxyhemoglobin.

Variation in CBF–$CMRO_2$ coupling is the second effect that could produce a different BOLD signal for the same underlying change in neural activity. Since CBF increases blood oxygenation and $CMRO_2$ decreases blood oxygenation, driving the

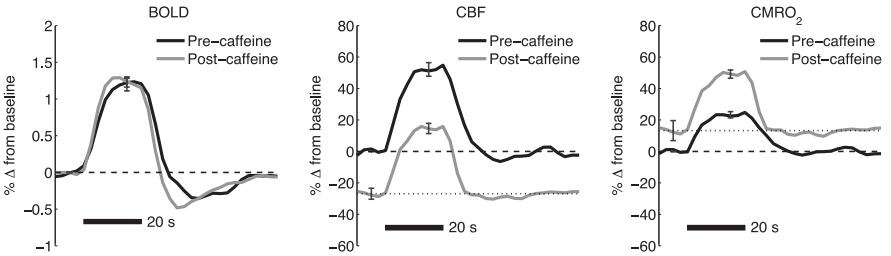


**Fig. 9.4** The physiological effects of a drug can be masked if one only looks at the BOLD response to a standard stimulus pre- and post administration of the drug. In this example, both the baseline shifts and the response to a visual stimulus were measured before and after caffeine administration with a calibrated BOLD experiment referring all changes to the pre-caffeine baseline state. Although the BOLD responses were similar *(left panel)*, the caffeine had significant effects on the underlying physiology *(middle* and *right panels)* that had counteracting effects on the BOLD response: *M* was increased but *n* was decreased. That is, the shift in the baseline, with decreased CBF paired with increased $CMRO_2$, would increase baseline deoxyhemoglobin. A second effect of the caffeine, though, was that the $CMRO_2$ response to the visual stimulus increased, reducing the CBF/$CMRO_2$ coupling ratio (Perthen et al. 2008; Griffeth and Buxton 2010b)

BOLD response in opposite directions, the resulting signal is a balance of these competing effects. Therefore, the magnitude of the signal change depends on the CBF/$CMRO_2$ coupling ratio, *n*, which is defined as the ratio of the fractional change in CBF to the fractional change in $CMRO_2$. If *n* were fixed for all neural responses, the coupling ratio would not have an impact on interpreting the BOLD response, but this is not the case as shown by numerous studies examining the dynamics of CBF and $CMRO_2$ (Ances et al. 2008; Chen and Parrish 2009; Herman et al. 2009; Moradi and Buxton 2011). For example, Fig. 9.3b shows three different response ratios for CBF and BOLD for a fixed $CMRO_2$ using the Davis model (Davis et al. 1998) to simulate the BOLD response. Assuming that $CMRO_2$ reflects underlying neural activity, this demonstrates how variations in the coupling of CBF and $CMRO_2$ affect the BOLD signal for the same underlying change in neural activity. These simulated data isolate how a change in the coupling ratio affects the BOLD signal, but a more complex relationship was recently demonstrated when changes occurred in both the baseline state and the coupling parameter. In this experiment, it was shown that caffeine administration decreased both baseline CBF and the coupling ratio between CBF and $CMRO_2$ (Griffeth and Buxton 2011b). The combined effect produced no measureable change in the BOLD signal response (Fig. 9.4). These examples emphasize the importance of quantifying the BOLD signal to assess oxygen metabolism.

## *Modeling the BOLD Response*

The Davis model was originally derived as a basic biophysical model of the BOLD signal's dependence on deoxyhemoglobin content (Davis et al. 1998). Vessels

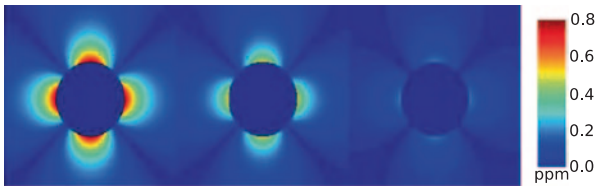


**Fig. 9.5** Simulation of the frequency offset due to a cylindrical blood vessel parallel to the magnetic field. Three blood oxygenation fractions were simulated, $Y=0.8$, 0.5, 0.2 *(left–right)*

containing paramagnetic deoxyhemoglobin are surrounded by diamagnetic tissue. This susceptibility difference causes microscopic field gradients to be produced surrounding the vessels (Fig. 9.5), causing the rate of decay of tissue protons ($R_2$*) that experience them to be increased. Modeling of this effect, through analytical and numerical means, has shown that the resulting change in extravascular $R_2$* ($\delta R_2$*) is a function of venous CBV, *CBVv*, and deoxyhemoglobin concentration, [*dHb*] (Yablonskiy and Haacke 1994; Boxerman et al. 1995; Ogawa et al. 1993);

$$R_2' = A \cdot \mathrm{CBV}v \cdot [\mathrm{dHb}]_v^{\beta}, \tag{9.2}$$

where $A$ is dependent on magnetic field strength and vessel geometry and $\beta$ reflects the length scale of the vessels involved, where $\beta=1$ for large vessels and $\beta=2$ for small vessels (Ogawa et al. 1993). Davis et al. performed additional Monte Carlo simulations to determine the correct value of $\beta$ for 1.5 T and suggested a value of 1.5.

The BOLD signal change may be expressed as a change in $R_2^*$ between activated and rest states ($\Delta R_2^*$), and, for small changes in the relaxation rate, this function may be linearized (Hoge et al. 1999):

$$\frac{\Delta S}{S_0} = \mathrm{e}^{-\mathrm{TE}\cdot\Delta R_2^*} - 1 \cong -\mathrm{TE}\cdot\Delta R_2^* \cdot \tag{9.3}$$

Since the $R_2$ of tissue is independent of blood oxygenation, $\Delta R_2$* is the difference in $\delta R_2$* contribution to $R_2$* between the activated and rest (subscript 0) conditions.

$$\Delta R_2^* = A \cdot CBV_v \cdot [dHb]_v^{\beta} - A \cdot CBV_{v0} \cdot [dHb]_{v0}^{\beta} \tag{9.4}$$

Substituting for $\Delta R_2$* into Eq. (9.3) leads to:
Equation 9.4 describes the basic physiological changes that underlie the BOLD response, including the effect of baseline deoxyhemoglobin content. This baseline effect is incorporated in a constant $M = \mathrm{TE}\cdot A\cdot \mathrm{CBV}_{v0}\cdot[\mathrm{dHb}]_{v0}^{\beta}$ and represents the maximum signal change, otherwise known as the "ceiling effect" (Buxton 2010).

In addition, CBF may be substituted for CBV in Eq. 9.4, assuming a power–law relationship $\mathrm{CBV} = k\cdot\mathrm{CBF}^{\alpha}$, where $\alpha=0.38$ (Grubb et al. 1974). Similarly,

following Fick's principle, it is possible to describe [dHb] as a function of CBF and $CMRO_2$. The final form of the Davis model can then be formed:

$$\frac{\Delta S}{S_0} = M \cdot \left[ 1 - \left( \frac{CBF}{CBF_0} \right)^{\alpha - \beta} \cdot \left( \frac{CMRO_2}{CMRO_{20}} \right)^{\beta} \right]. \tag{9.5}$$

This model demonstrates how the BOLD signal is defined as a basic dependence on CBF, which is modulated by the maximum signal change ($M$) and CBF–$CMRO_2$ coupling. In the context of the previous section, $M$ represents the "ceiling effect"; the maximum signal change that would occur if the venous blood is 100 % oxygenated.

## A Multimodal Approach: Adding CBF and CBV Measurements

Due to the numerous confounding factors in BOLD interpretation, a multimodal approach is needed for determining $CMRO_2$. While the complexity of the BOLD signal creates difficulty in interpreting experimental results, it becomes advantageous when BOLD is combined with dynamic CBF and/or CBV measurements. This combination allows investigation of $CMRO_2$ dynamics when interpreted within an appropriate mathematical framework (Davis et al. 1998; Lin et al. 2008; Buxton 2010). As such, these complementary measures may be separated into two general categories: those that measure CBF and those that measure CBV.

### *Cerebral Blood Flow*

ASL is a term applied to a collection of techniques developed to isolate and quantify the component of the MR signal that is derived from inflowing arterial blood. Many perfusion-sensitive techniques have been created since the development of the first ASL method in 1992 (Detre et al. 1992), and each possesses a unique set of features designed to address one or several of the challenges associated with measuring CBF. For a detailed description of ASL methodology, refer to Chap. 11. However, in the context of quantifying fMRI, it is important to consider several systematic errors that may occur in ASL that must be accounted for if accurate measurements of CBF are to be made (Wong et al. 1997). The ability to quantify blood flow precisely in physiological units is very useful for tracking cerebral perfusion over long periods of time and may prove to be effective for monitoring diseases in which the cerebral vasculature is impaired; thus, the improvement of ASL pulse sequences and models remains an active area of functional imaging research (Petersen et al. 2006; Francis et al. 2008; Dai et al. 2008).

Each of these sources of error results from properties of the magnetically tagged "bolus" of blood. Full inversion of this arterial blood is assumed, but this is generally not the case, especially at the leading and trailing edges of the bolus. If the tagging "efficiency" is not properly accounted for, then the delivery of blood to the imaging volume may be underestimated. Second, the inversion pulse may have off-resonance effects on the imaging volume, reducing the signal of the static tissue in the "tagged" images. To compensate for this, the control image must be carefully designed to have the same off-resonance effects.

Another source of error results from the inherently transitory nature of the ASL labeling process. Once tagged, arterial blood does not remain inverted indefinitely, but begins to relax at a characteristic rate ($1/T_1$). The longer one waits to acquire an image (longer TI), the more the inverted blood will relax, reducing the magnitude of the difference signal. This process is further complicated by the fact that labeled spins in arterial blood do not relax at the same rate ($1/T_1$) as spins that have diffused into the tissue. If the tagged spins spend a significant portion of the time TI in the tissue compartment, one must take into account the differing $T_1$ times for tissue and blood.

A key requirement of any ASL sequence is to produce a bolus of tagged blood with a well-defined temporal width and that the timing of the sequence allows for all of the tagged blood to be delivered to all elements of tissue by the time of measurement. An important problem in meeting the latter requirement is the variability of the transit delay time of the arterial blood—the time required for the blood to move from the tagging region to the capillaries of the imaging volume. If the TI is not long enough to allow all of the tagged blood to enter the tissue, then regional CBF will be underestimated. Unfortunately, the transit delay is not uniform across the head, requiring that one account for this variability in multi-slice imaging. Finally, the process of dynamic subtraction significantly reduces the signal-to-noise ratio of a perfusion-weighted image, decreasing the sensitivity of an ASL experiment to activation and potentially introducing error into calculations of CBF.

When these effects are properly taken into account, either through pulse sequence design or through modeling, ASL provides a means to calculate CBF in physiological units. In addition, fractional changes in CBF can be measured by taking the ratio of the difference signal acquired during active and baseline conditions. Such measurements are not dependent on tagging efficiency, as long as a sharply defined bolus can be created and the effects of transit delay controlled for. When combined with measurements of CBV, even this semi-quantitative ASL may be used to estimate physiological parameters from BOLD-weighted images.

## *Cerebral Blood Volume*

Noninvasive MRI techniques designed to measure changes in CBV attempt to isolate the signal originating in the vascular compartment from that of the tissue compartment. In order to accurately quantify the BOLD signal, the blood volume must be further differentiated into those components that contain deoxygenated blood

and those that do not. Herein lies the problem, and it has proven to be more difficult to solve than tracking changes in CBF. While the first MRI techniques to measure CBV (Villringer et al. 1988) predate both BOLD (Ogawa et al. 1990) and ASL (Detre et al. 1992) methods, the majority of CBV measurement techniques are sensitive to the total blood volume, that is, arterial, capillary, and venous. In humans, these methods include gadolinium-based contrast agent methods (Belliveau et al. 1991; Pears et al. 2003) as well as endogenous contrasts such as vascular space occupancy (VASO; Lu et al. 2003). If the CBV changes are proportionately larger on the arterial side, these techniques have the potential to overestimate the contribution of venous blood volume changes to the BOLD response.

A detailed description of the VASO method is provided in Chap. 11. However, it is still important to consider sources of systematic error that may influence the quantification of the fMRI signal. The measured VASO signal is sensitive to the "absolute" change in CBV, whereas it is the "fractional" change in CBV that is relevant to interpreting the BOLD response. A fractional change in CBV cannot be determined from the VASO signal alone, and a value for the baseline must be assumed (Donahue et al. 2006). Therefore, unlike the ASL signal where the fractional change in CBF can be calculated from the data, a measurement of fractional CBV made using the VASO technique requires an assumed value of resting CBV.

If the CBV change with activation is proportional across all vascular compartments, then using a measurement of total CBV such as VASO could potentially be used to estimate the venous CBV change for modeling the BOLD response. However, recent studies suggest that arteriolar dilation may greatly exceed venous dilation in the vasculature of stimulated cerebral cortical tissue (Lee et al. 2001; Kim and Kim 2006; Hillman et al. 2007; Kim et al. 2007) and may thus contribute significantly to the changes in CBV measured by VASO. In this case, VASO will tend to overestimate the CBV changes relevant to BOLD modeling and underestimate changes in $CMRO_2$.

To address this challenge, techniques such as the venous refocusing for volume estimation (VERVE) have been developed (Stefanovic and Pike 2005). The VERVE technique is based upon the observation that the $T_2$ measured using a Carr–Purcell–Meiboom–Gill (CPMG) pulse sequence is dependent on the spacing of the 180° refocusing pulses, otherwise known as $\tau_{CP}$. In a similar manner to the extravascular BOLD signal, the susceptibility difference between deoxygenated red blood cells and the surrounding blood plasma causes microscopic field gradients to be produced. Plasma spins surrounding the red blood cells experience this field offset causing a loss of phase coherence manifested as an enhanced rate of signal decay. As the distance traveled by any given spin is of a similar scale to the red blood cell, the spin will experience a large number of field offsets leading to a loss of spin history. Phase acquired in this way cannot be recovered with a traditional spin echo. However, if multiple refocusing pulses are employed with a sufficiently short $\tau_{CP}$, then the accrued phase can be recovered before the spin has traveled too far from its current position. In the limit of infinitely short $\tau_{CP}$, all phase would be recovered and $T_2$ would be maximized. The VERVE method exploits this sensitivity to $\tau_{CP}$ by employing fast and slow refocusing pulse trains to measure the signal intensity at a

single effective echo time (TE). Images are acquired in an interleaved fashion and are subtracted pair wise in a manner similar to ASL. Since the tissue does not have any small-scale susceptibility inclusions, the fast and slow regimes have the same effect and are subtracted out. What remains is a signal that is a function of venous CBV and the change in blood $T_2$ between rest and activation. To convert this relative VERVE signal into a fractional change in CBV requires assumptions about the oxygen saturation of venous blood in baseline and active states (Stefanovic and Pike 2005). As was the case with VASO, estimates of such parameters may be obtained from the literature. However, these values may not always be applicable to every subject, and even small variations in the values of these estimated parameters may have large effects on the calculation of CBV. Measurements using VERVE suggest a lower value of Grubb's constant when relating CBF and venous CBV. For visual stimulus-driven changes in flow, $\alpha = 0.23$ was reported and for hypercapnia a value of $\alpha = 0.18$ (Chen and Pike 2009, 2010). These results are consistent with the idea that venous CBV increases to a lesser degree than total CBV.

## Measuring Steady-State $CMRO_2$

### *TRUST*

In principle, the simplest way to measure $CMRO_2$ would be to exploit the blood oxygenation dependence of $R_2$. This relationship has been well studied and has been shown to be quadratically dependent on the deoxyhemoglobin content (Spees et al. 2001; Silvennoinen et al. 2003). However, the blood represents a relatively small volume fraction of the standard imaging voxel and, so, in the cortex, the measured signal is a mixture of tissue and blood signals. It is not possible to merely measure the $R_2$ of an area of cortex and convert this to oxygenation using a calibration curve generated from ex vivo blood samples. In fact, it is difficult to measure a pure blood signal in large venous vessels, such as the sagittal sinus, using standard sequences.

Recently, a pulse sequence was developed to remove the sensitivity of existing methods to background tissue signal. This method is based on the Proximal Inversion with a Control for Off-Resonance Effects (PICORE) ASL technique and is known as TRUST ((Lu and Ge 2008). In conventional PICORE ASL, the aim is to magnetically tag arterial blood using an inversion pulse in vessels inferior to the volume of interest and image this blood as it flows into this region. A control image, in which the arterial blood is not inverted, is also acquired, and the subtraction of these images is used to isolate the blood signal. In the TRUST method, the tagging plane is placed superior to the volume of interest in order to tag venous blood in the sagittal sinus as it flows back towards the heart. By subtracting tag and control images, the venous blood is isolated. Images are acquired with different degrees of $T_2$ weighting, which is applied using a train of nonselective $T_2$ preparation pulses (Brittain et al. 1995) rather than a conventional spin echo. This preparation module follows the principles of the CPMG sequence and is used to acquire images at echo

times between 0 and 160 ms, while retaining a fixed refocusing interval, $\tau_{CP}$. Following subtraction, these data can be fitted for $T_2$, although the $T_1$ recovery of the tagged blood must also be taken into account. The resultant $T_2$ value is then converted to an oxygenation value using a calibration curve (Silvennoinen et al. 2003). This enables the OEF of the whole brain to be assessed by measuring venous blood oxygenation in a large draining vein such as the sagittal sinus.

Although the TRUST method allows the oxygenation of blood to be measured, it cannot measure $CMRO_2$ on its own. However, restating Fick's principle that $CMRO_2$ is the product of blood flow and arteriovenous oxygen difference, it is possible to use this measurement to calculate the absolute $CMRO_2$ of the whole brain. Hence, the $CMRO_2$ can be modeled in the following way:

$$\mathrm{CMRO_2} = \mathrm{CBF}(Y_\mathrm{a} - Y_\mathrm{v})C_\mathrm{a}, \tag{9.6}$$

where $Y_a$ and $Y_v$ are the arterial and venous blood oxygenation saturations and $C_a$ represents the oxygen-carrying capacity of the blood. In a recently described method, this approach was followed by measuring venous oxygenation saturation in the sagittal sinus by combining TRUST and measuring CBF measurements using a phase-contrast method (Xu et al. 2009). Blood oxygenation has alternatively been measured by an MR susceptometry technique (Jain et al. 2010). In both cases, a phase-contrast approach was chosen to give a whole-head CBF measurement that is comparable with the oximetry measurement. While ASL is good at measuring spatial variations in CBF, phase-contrast MRI in the feeding arteries gives a better estimation of whole-head CBF. Phase contrast provides a measure of blood velocity that must be multiplied by the vessel's cross-sectional area to measure blood flow. Further normalization by the intracranial volume, calculated from anatomical images, yields the whole-head CBF. Equation 9.2 can then be applied using literature values for $C_a$ and assuming that arterial blood is 100% oxygenated ($Y_a = 1$). This method has been shown to give whole-head $CMRO_2$ results that are comparable with PET literature values (Mintun et al. 1984; Xu et al. 2009).

New methods are emerging which take this approach one step further by attempting to measure venous $T_2$ at the tissue level rather than in the large draining vessels (Bolar et al. 2009; Guo and Wong 2010). This presents a host of problems including an inherently low signal-to-noise ratio due to the small volume fraction occupied by the venular blood. An approach such as TRUST fails for the tissue compartment as in order to tag the blood entering the venules the arterial blood will inevitably also be tagged. Therefore, an appropriate method must isolate the venular blood, while suppressing the signal from tissue and large arterial and venous vessels. In the QUIXOTIC approach, velocity-selective (VS) excitation is used to provide large vessel suppression, while a two-phase tag and control acquisition is used to remove the tissue signal (Bolar et al. 2009). VS pulses are used to saturate the signal from spins flowing above a cutoff velocity, $V_{cut}$. This cutoff frequency is set to 1 cm $s^{-1}$ to saturate the spins contained within the arteries, arterioles, venules, and veins. Two VS pulses are applied separated by an inflow time, TI. Application of the first VS pulse saturates all of the blood except that contained within the microvasculature.

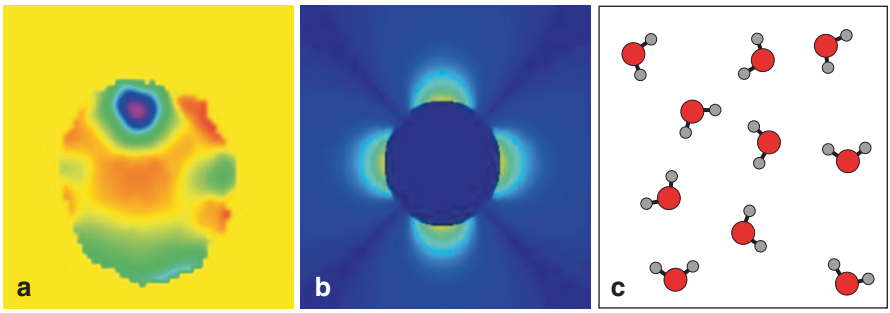


**Fig. 9.6** Three regimes of the qBOLD model. **a** Macroscopic field inhomogeneity due to magnetic field variation on the scale of the head. **b** Mesoscopic effects due to field gradients surrounding deoxygenated blood vessels. **c** Microscopic effects due to dipole–dipole relaxation and diffusion of spins

In the tag phase, a second identical VS pulse is applied, which saturates any of the remaining microvascular blood that has moved into the venular space. For the control image, this is replaced by a dummy VS pulse. On subtraction of these images, the tissue signal and the signal from the blood that remains in the microvasculature are removed, isolating the venular blood signal. Images are then acquired with different degrees of $T_2$ weighting using the same $T_2$ preparation module as is used in TRUST (Brittain et al. 1995). When combined with a local measurement of CBF using ASL, the local resting $CMRO_2$ can be calculated.

## *Quantitative BOLD*

The qBOLD method seeks to measure OEF and venous blood volume by exploiting the characteristics of the gradient-echo signal (Yablonskiy 1998). The processes which lead to the decay of this signal can be divided into three categories: microscopic, mesoscopic, and macroscopic (Fig. 9.6). Each of these processes reflects the relative length scale over which they act with respect to the voxel dimensions.

The microscopic scale reflects the effect of spin–spin relaxation, otherwise known as $T_2$ decay. This inherent property of tissue cannot be reversed by the use of a 180° refocusing pulse and is modeled as a mono-exponential decay. The mesoscopic and macroscopic processes act to increase the rate of relaxation by $R_2'$ and are caused by magnetic field inhomogeneity. In the case of the macroscopic process, the scale of the field inhomogeneity is large relative to the voxel size. This inhomogeneity is caused by the head when placed in the magnet of the MRI scanner. Ordinarily, the magnet has a very high magnetic field homogeneity (<0.1 ppm), but it is disturbed by the differences in susceptibility within the head and between the head and the surrounding air. Shimming is used to mitigate this effect, but field gradients will always remain at air–tissue interfaces. These gradients cause an offset with respect to the main magnetic field causing spins across the voxel to precess at

a range of frequencies. As the spins are relatively static in this large-scale inhomogeneity, they accrue phase at a rate that is proportional to the local field offset. The distribution of phases is then dependent on the distribution of magnetic field offsets in the voxel. Typically, these field offsets can be described by a constant gradient across the voxel. In this case, the effect of macroscopic field inhomogeneity can be described by a *sinc* function. However, for small field inhomogeneities, this can be approximated by a Gaussian (Yablonskiy 1998):

$$\left|F(t)\right| = \exp(-a \cdot t^2) \quad where\, a = \frac{\Delta\omega^2}{24} \tag{9.7}$$

where $t$ is the echo time and $\Delta\omega$ is the frequency offset. The signal measured in an experiment is then the product of the sub-voxel signal decay and the macroscopic decay, $|F(t)|$, which can be removed by fitting Eq. 9.7 to the measured signal. The final process, the mesoscopic scale, is the most important in the context of the qBOLD method. This effect is intermediate in scale between the microscopic and macroscopic processes and is due to the blood vessels. As described earlier, the susceptibility difference between vessels and tissue causes microscopic field gradients to be formed. In a similar manner to the macroscopic inhomogeneity effect, tissue spins surrounding the vessels experience this field offset, and their rate of decay is enhanced. The prototypical qBOLD experiment is based on a spin-echo acquisition with echo time TE. The mesoscopic signal is assumed to be in the static dephasing regime, and it is therefore refocused by the 180° pulse. This equates to a vessel scale that is approximately 7 μm and greater and reflects venular vessels and larger.

Theoretical investigations of the static dephasing signal around magnetized cylinders have shown that the temporal characteristics of the decay are time dependent and fall into two time scales: short and long (Yablonskiy 1998). The relevant time scale can be determined with reference to the characteristic time, $t_c$;

$$t_c^{-1} = \delta\omega = \frac{4}{3}\pi \cdot \omega_0 \cdot \Delta\chi \cdot [\mathrm{dHb}], \tag{9.8}$$

where $\omega_0$ is the Larmor angular frequency, $\Delta\chi$ is the molar susceptibility difference between fully oxygenated and deoxygenated red blood cells, and [dHb] is the concentration of deoxyhemoglobin. This characteristic time is dependent on $\delta\omega$, which is the characteristic variation in precession frequency around randomly distributed magnetized cylinders, and reflects local field offsets experienced by tissue spins. Equation 9.8 can be broken down into components that reflect the geometry ($4\pi/3$), magnetic field strength ($\omega_0$), and the susceptibility difference ($\Delta\chi \cdot [\mathrm{dHb}]$). Figure 9.7 describes the relevant time scales for a spin-echo sequence and plots the signal decay, $S_{meso}$, due to $R_2'$ on a logarithmic scale. As the signal comes back into focus, prior to the spin echo, $R_2'$ is negative. Application of the refocusing pulse causes the phases of the spins to begin to converge after they were formerly

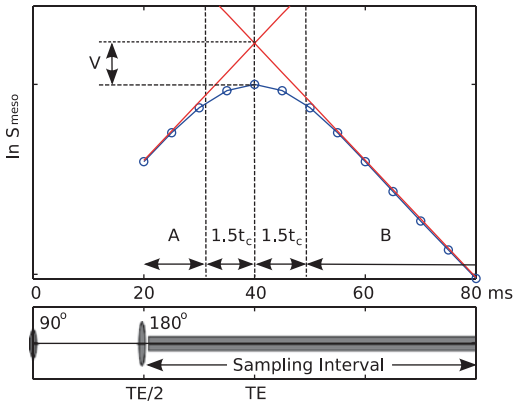


**Fig. 9.7** Schematic of mesoscopic signal decay *(circles)* with the long time regime extrapolated to $t = \mathrm{TE}$ *(straight lines)*

diverging due to local field offsets in the voxel. This leads to differing values of $R_2^*$ measured prior, $R_{2-}^*$, and subsequent to, $R_2^*$, the spin echo.

$$R_{2-}^* = R_2 - R_2' \tag{9.9}$$

$$R_{2-}^* = R_2 + R_2' \tag{9.10}$$

For the short time scale, where data acquisition is within $1.5t_c$ of the spin-echo formation, the signal decay due to the mesoscopic effect is quadratically exponential. During the long time scale (intervals A and B) the mesoscopic contribution to signal is linearly exponential. To simplify fitting these effects can be summarized by two quadratic equations:

$$\ln(S(t)) = c_1 - b_1 \cdot (t - \mathrm{TE}) - a_1 \cdot (t - \mathrm{TE})^2 \text{ for interval A,} \tag{9.11}$$

$$\ln(S(t)) = c_2 - b_2 \cdot (t - \mathrm{TE}) - a_2 \cdot (t - \mathrm{TE})^2 \text{ for interval B.} \tag{9.12}$$

Here, the parameter $c$ is the intercept at TE, $b_1$ and $b_2$ are $R_{2-}^*$ and $R_2^*$, respectively, and $a$ is the contribution of macroscopic field inhomogeneity. For a simple model system consisting of a single tissue type, and where the intravascular signal contribution can be ignored, Eqs. 9.11 and 9.12 can be fitted to signal decay data to calculate the venous blood oxygenation and venous volume (Yablonskiy 1998). Data are commonly acquired using the gradient-echo sampling of spin-echo (GESSE) method. Gradient-echo data are acquired around the spin echo formed by a 180° refocusing pulse. Rather than acquiring each image using a single-shot technique, each repetition of the sequence acquires a single line of $k$-space at many closely spaced echo times. Each repeat increments the phase encoding to cover $k$-space. The values of $R_2'$ and $S(\mathrm{TE})$ are calculated from the fitted parameters $c_{1,2}$ and $b_{1,2}$.

$$R_2^{'} = \frac{b_2 - b_1}{2} \tag{9.13}$$

$$S_{\text{fit}}(\text{TE}) = \frac{c_1 + c_2}{2} \tag{9.14}$$

These values can then be used in combination with the signal measured at TE, $S_{\text{meas}}(\text{TE})$, to calculate the venous volume, $V$, and the deoxyhemoglobin concentration.

$$V = \ln(S_{\text{fit}}(\text{TE})) - \ln(S_{\text{meas}}(\text{TE})), \tag{9.15}$$

$$[\text{dHb}] = \frac{3}{4} \frac{R_2}{\pi \cdot \omega_0 \cdot V \cdot \Delta\chi} \tag{9.16}$$

However, in reality, this model is an oversimplification, since each imaging voxel has signal contributions from components other than gray matter (He and Yablonskiy 2007). In the GESSE implementation of this method, isolation of the mesoscopic signal is made more difficult if the underlying $R_2$ decay is multiexponential. This would occur if, due to the partial volume effect, the voxel contains both gray matter and CSF. As each of these components has a significantly different $R_2$, the resulting signal decay is biexponential. Additionally, intravascular signal is not included in the simple model, despite it providing a significant contribution to the BOLD signal at 3.0 T and below. Studies that incorporate all of these effects have been performed and yield results that are comparable with the PET literature (He and Yablonskiy 2007). However, in fitting such a high-dimensional model, a great deal of care must be taken to select reasonable starting conditions for the optimization procedure.

Experiments performed using asymmetric spin-echo (ASE) measurements with diffusion weighting attempt to address the issue of multiexponential $R_2$ decay (An and Lin 2003). ASE measurements are also based on a spin-echo pulse sequence, but with the spin echo shifted from the gradient echo that defines the sampling of the center of $k$-space. Images are acquired at a single TE, but the timing of the 180° pulse is shifted towards the origin by a time $\tau$. This causes the spin echo to form at a time $2\tau$ before TE, resulting in an additional degree of $R_2'$ weighting. However, since the images are acquired at the same TE, all of the images have the same $R_2$ weighting and the $R_2$ contribution does not need to be subtracted out as in Eq. 9.13. Images are acquired with a range of $\tau$ values using a single-shot acquisition rather than a segmented approach. In addition, rather than modeling the intravascular signal, as has been proposed using the GESSE method (He and Yablonskiy 2007), the application of bipolar diffusion gradients causes the signal of flowing spins to be suppressed. However, while the ASE method mitigates the effects of multiexponential decay and intravascular signal, it may introduce another problem. This problem is caused by spins in the diffusion-narrowing regime. It is well known that in a CPMG

sequence, the diffusion effect on $T_2$ is dependent on the spacing of the 180° refocusing pulses. As the ASE shifts the 180° pulse closer to the excitation, the degree to which diffusion affects the signal will be reduced. Therefore, this may introduce a signal dependency on the value of $\tau$, as multiple values are used in this sequence.

The qBOLD method provides quantitative values of OEF and venous CBV at the tissue level. This does not require an injection of contrast agent as endogenous BOLD contrast is used, enabling repeated measurements to be performed. Each of the data acquisition methods has their own advantages and disadvantages. The ASE approach benefits from simplicity in the fitting of the data by trying to remove unwanted signals during data acquisition, whereas the GESSE approach attempts to model these signals and remove them by fitting to the data. When combined with CBF, calculations of $CMRO_2$ can also be made with potential applications both in the clinic and in basic physiology.

## Measuring Dynamic $CMRO_2$ Changes with Calibrated BOLD

### *Hypercapnic Calibration*

The aim of the calibrated BOLD method is to combine the information provided by CBF measurements with the information contained within the BOLD (Davis et al. 1998). This enables the change in $CMRO_2$ to be measured with respect to a resting baseline (Perthen et al. 2008). As has been described earlier, the BOLD response is a balance of competing effects. Increased blood flow reduces the OEF causing the venous blood to become more oxygenated, while increases in metabolism act in the opposite sense to reduce blood oxygenation. In the healthy brain, the CBF effect dominates, determining the sign of the BOLD response, but the magnitude of the BOLD response is strongly modulated by the $CMRO_2$ response.

The calibrated BOLD method relies upon the Davis model of the BOLD signal (Eq. 9.5), which is described in detail in the BOLD modeling section of this chapter. The constant $M$ reflects the baseline state of metabolic activity and also the maximum amplitude of the positive BOLD response. This would occur if the venous blood became 100% oxygenated ([dHb] = 0) causing the BOLD contrast to be nulled. The basic idea of the calibrated BOLD method is that if $M$ is known for an activated region, then measurements of the CBF and BOLD responses during activation can be combined with Eq. 9.5 to calculate the fractional change in $CMRO_2$ during the activation. It is important to note that the value of $M$ depends on aspects of both local anatomy and physiology, such as baseline venous blood volume and OEF, and also on details of the experiment, such as echo time and field strength. Therefore, to measure stimulus-induced changes in $CMRO_2$, a calibration experiment must first be performed to measure $M$. Experiments to measure $M$ directly

have been performed, but are not generally used due to the high levels of carbon dioxide required to induce such large changes in blood flow (Gauthier et al. 2010).

In practice, $M$ is calculated from Eq. 9.5 by modulating the deoxyhemoglobin concentration of the venous blood, while leaving the resting $CMRO_2$ unchanged. Traditionally, this is achieved by presenting the subject with air containing a small percentage of carbon dioxide. This induces hypercapnia in the subject causing an increase in CBF, which reduces [dHb] and increases CBV. Mild hypercapnia is not thought to affect resting $CMRO_2$ and so this stimulus is considered isometabolic. The measured BOLD response is then:

$$\frac{\Delta S}{S_0} = M \cdot \left[ 1 - \left( \frac{\mathrm{CBF}}{\mathrm{CBF}_0} \right)^{\alpha - \beta} \right] \tag{9.17}$$

In practice, the hypercapnic gas mixture is presented as several long blocks, interleaved with room air, while images are acquired using a combined ASL and BOLD pulse sequence. Functional data are also acquired using the same pulse sequence. The calibration constant is then calculated from the relative changes in BOLD signal and CBF from the calibration run for a functional region of interest (ROI). This value of $M$ can then be applied to the data from the functional run to calculate the change in $CMRO_2$ associated with the activation.

## *Hyperoxic Calibration*

In response to concerns about whether mild hypercapnia alters $CMRO_2$, an alternative calibration method was proposed recently that replaces carbon dioxide with air enriched with oxygen (Chiarelli et al. 2007b). Rather than modulate [dHb] indirectly by increasing flow, hyperoxia affects the venous blood oxygenation directly. At normoxia, the hemoglobin of arterial blood is nearly 100 % saturated with oxygen. However, additional oxygen may still be carried by the plasma, as this is linearly proportional to the oxygen partial pressure ($PO_2$) of the inspired gas. During hyperoxia, venous hemoglobin saturation increases as the additional oxygen carried in the plasma results in less desaturation due to resting metabolic oxygen consumption.

$$\frac{\Delta S}{S_0} = M \cdot \left[ 1 - \left( \frac{\mathrm{CBF}}{\mathrm{CBF}_0} \right)^{\alpha} \cdot \left( \frac{[\mathrm{dHb}]_v}{[\mathrm{dHb}]_{v0}} + \frac{\mathrm{CBF}_0}{\mathrm{CBF}} - 1 \right)^{\beta} \right] \cdot \tag{9.18}$$

Note that if there was no change in CBF with hyperoxia, the measured BOLD signal change would depend just on $M$ and the change in venous deoxyhemoglobin concentration. Provided one can estimate this venous deoxyhemoglobin change, one could calculate $M$. In practice, it has been shown that hyperoxia can cause vasoconstriction and hence a reduction in flow, so that CBF measurements also are required, typically using ASL (Bulte et al. 2007). However, flow measurements using ASL

are confounded by the change in arterial $T_1$ caused by an increased plasma oxygen concentration. Corrected flow data can be used in conjunction with Eq. 9.18 to account for hyperoxia-induced flow reductions (Bulte et al. 2007).

The change in deoxyhemoglobin concentration must also be calculated based on the arterial $PO_2$ ($PaO_2$) using the principles of oxygen transport. The value of $PaO_2$ is inferred from measurements of end-tidal $PO_2$ in mmHg, and its effect on arterial saturation, $SaO_2$, is calculated using the Severinghaus equation (Severinghaus 1979).

$$\mathrm{SaO_2} = \frac{1}{\frac{23,400}{(\mathrm{PaO_2})^3 + 150 \cdot (\mathrm{PaO_2})} + 1} \tag{9.19}$$

The calculated value of $SaO_2$ is then used to calculate the oxygen content of arterial blood during hyperoxia, $CaO_2$,

$$\mathrm{CaO_2} = \phi \cdot [\mathrm{Hb}] \cdot \mathrm{SaO_2} + \varepsilon \cdot \mathrm{PaO_2}, \tag{9.20}$$

where $\varphi$ is the oxygen-carrying capacity of hemoglobin (1.34 $ml_{O_2}/g_{\mathrm{Hb}}$), [Hb] is the concentration of hemoglobin in the blood (assumed to be 15 $g_{Hb}/dl_{blood}$), and $\varepsilon$ is solubility of oxygen in plasma (0.0031 $ml_{O_2}/(dl_{blood} \cdot mmHg)$) (Chiarelli et al. 2007b). Assuming that the amount of oxygen extracted (OEF) for metabolism is constant during hyperoxia, the venous oxygen content, $CvO_2$, can be calculated.

$$\mathrm{CvO_2} = \mathrm{CaO_2} - \mathrm{CaO_{20}} \cdot \mathrm{OEF} \tag{9.21}$$

The normoxic oxygen content, $CaO_{20}$, is calculated using Eq. 9.20 and combined with the preceding results to calculate the change in venous oxygen saturation, $SvO_2$.

$$\mathrm{SvO_2} = \frac{\mathrm{CvO_2} - \varepsilon \cdot \mathrm{PvO_2}}{\phi \cdot [\mathrm{Hb}]} \tag{9.22}$$

Chiarelli et al. assume that $PvO_2$ is small enough to be neglected. That is, the extra $O_2$ carried in arterial plasma is quickly lost to tissue, so that venous $O_2$ has the normal distribution in which only a few percent is present as dissolved gas and the rest is bound to hemoglobin. Finally, assuming that the hematocrit does not change during hyperoxia, the change in [dHb] is calculated as:

$$\frac{[\mathrm{dHb}]_v}{[\mathrm{dHb}]_{v0}} = \frac{1 - \mathrm{SvO_2}}{1 - \mathrm{SvO_{20}}}. \tag{9.23}$$

In summary, the extra oxygen carried by the arterial blood during hyperoxia is calculated from measured end-tidal $PO_2$ values. Assuming that the amount of oxygen consumed by metabolism remains the same, this value is then used to calculate the change in venous oxygen saturation. In addition, it is assumed that $P_{ET}O_2$ accurately reflects $PaO_2$, venous $PO_2$ is small enough to be ignored, and that the blood hematocrit does not change.

An additional consideration when performing a respiratory challenge is the interdependency of changes in arterial concentrations of oxygen and carbon dioxide (Wise et al. 2007; Prisman et al. 2008). Independence of these changes is particularly important for hyperoxia experiments due to the relatively weak effect of oxygen on the BOLD signal. A change in arterial $PO_2$ of the order of 200 mmHg would result from an $F_IO_2$ of 0.5 causing a BOLD signal change of ~1.2% (Prisman et al. 2008). Presentation of oxygen is often accompanied by a reduction in carbon dioxide $PO_2$. A change in arterial $PO_2$ of just 1 mmHg causes a BOLD signal change of ~0.4% (Prisman et al. 2008). Since these effects act in opposing directions, presentation of oxygen without controlling $PCO_2$ could easily lead to cancellation of the oxygen effect. Fortunately, in the case of hypercapnia calibration, the relative insensitivity to oxygen changes means that an increased $PO_2$ due to mild hyperventilation has little effect on the BOLD signal. It is also possible to control this effect by using a respiratory manipulation (Wise et al. 2007; Prisman et al. 2008).

## Current Issues with Calibrated BOLD

### *Do Hypercapnia and Hyperoxia Alter $CMRO_2$?*

The calibrated BOLD model is widely used, but validation of the method is still ongoing. Debate surrounds the methods used to measure *M* and how changes in CBV are determined. The effectiveness of the calibration experiment is dependent on the assumption that the respiratory challenge is isometabolic. If this was not the case, and there was a change in the resting metabolism, then an error in the value of *M* could be introduced. Recently, it has been shown that inhalation of air containing 5% $CO_2$ causes an appreciable reduction in resting metabolism (Xu et al. 2010b). Using a combination of TRUST and phase-contrast flow measurements, a 13.4% reduction in $CMRO_2$ was found. This is consistent with intracortical recordings that show a significant reduction in spontaneous neuronal activity during hypercapnia (Zappe et al. 2008). In this study, inhalation of 6% $CO_2$ resulted in an ~15% reduction in multiunit activity. However, because ventilation was fixed in these animal studies, while humans are able to increase ventilation and partially reduce the $PCO_2$ increase in the blood, the induced changes in $PCO_2$ may be higher than they would be in humans breathing the same gas mixture. Reduced stimulus-evoked $CMRO_2$ has also been reported for 10% $CO_2$ inhalation (Sicard and Duong 2005), but a reduction was not noted for more moderate hypercapnia. Reduced resting $CMRO_2$

would lead to an overestimation of $M$ when using hypercapnic calibration. For example, taking values from the literature (Perthen et al. 2008), a 13.4 % reduction in $CMRO_2$ during hypercapnia will cause $M$ to be overestimated by ~36 %. In turn, this will cause the stimulus-induced metabolism change to be overestimated by ~7 %. Similar measurements during hyperoxia with $F_IO_2 = 0.98$ have also been performed (Xu et al. 2010). These experiments measure a reduction in resting $CMRO_2$ of 11 %. This would lead to $M$ being underestimated in the hyperoxic calibration experiment. Although in practice much lower levels of oxygen are used, and assuming a linear reduction, hyperoxia would cause an ~4 % reduction in resting $CMRO_2$. This reduction in $CMRO_2$ would cause $M$ to be overestimated by ~16 % and stimulus-induced metabolism changes to be overestimated by ~3 %.

A recent comparison of hypercapnic and hyperoxic calibration methods provides some insight into this issue of isometabolism (Mark et al. 2011). The calibration constant $M$ was calculated for a range of hypercapnia and hyperoxia levels. For hyperoxia, where the authors suggest that isometabolism is more certain, differences in $M$ between the oxygen levels ($P_{ET}O_2 = 140$, 240, 340 mmHg) were statistically insignificant. However, for the range of carbon dioxide levels used ($P_{ET}CO_2 = 3$, 5, 7, 9 mmHg), $M$ was observed to increase systematically with $CO_2$. This may be additional evidence that $CMRO_2$ is reduced with hypercapnia.

## *How Large Are the Venous CBV Changes with Activation?*

The Davis model assumes a fixed relationship between total CBV and CBF (Grubb et al. 1974). The Grubb constant $\alpha$, which defines this relationship, was measured as a whole-head average at steady state (Grubb et al. 1974). This results in the calibrated BOLD model only being valid when both the calibration and functional stimuli are of a sufficient time duration for a steady state to be achieved. Experiments have shown that Grubb's constant is dependent on the phase of the BOLD response, that is, rise, plateau, or recovery phase (Kida et al. 2007). Recent studies have sought to measure changes in CBV to avoid assuming the Grubb relation and measure dynamic changes in $CMRO_2$ (Lin et al. 2008; Donahue et al. 2009). Measurements of the change in CBV were acquired using the VASO technique (Lu et al. 2003) and combined with simultaneous measurements of BOLD and CBF (Lin et al. 2008). This study found that increases in CBF were not matched by increases in $CMRO_2$, especially as stimulus frequency increases. This produces an increase in the CBF–$CMRO_2$ coupling parameter, $n$, consistent with PET studies (Vafaee et al. 1999; Vafaee and Gjedde 2000). Also, using VASO to measure CBV, another group found a similar coupling between CBF and $CMRO_2$ that is consistent with PET in both motor cortex ($n = 3.8$) and visual cortex ($n = 4.8$) (Donahue et al. 2009). On extrapolating the data of Lin et al., the effective Grubb constant is found to be $\alpha = 0.6$ using normalized CBF = 1.68 and normalized CBV = 1.38 (Lin et al. 2008). This is consistent with PET measurement of CBF–CBV coupling, where $\alpha = 0.64$ was measured for cortical gray matter (Rostrup et al. 2005). Unfortunately, the measurements of

CBV provided by the VASO technique are known to reflect total CBV, while the volume changes that underlie the BOLD response are predominantly due to volume change in the venous compartment. It has previously been assumed that since the venous blood volume is the dominant source of resting blood volume, this value of $\alpha$ would accurately reflect the venous volume change (Buxton et al. 1998). It has since been shown that although arterial blood volume is smaller than venous blood volume at rest, it increases to a proportionately larger degree during activation (Lee et al. 2001). Experiments using the VERVE technique, which is sensitive to venous blood volume changes, have measured $\alpha = 0.23$ and $\alpha = 0.18$ for visual stimulus and hypercapnia, respectively, in venous vessels (Chen and Pike 2009, 2010). Although these values for stimulus- and hypercapnia-induced changes in CBV are not significantly different, it remains a possibility that they could be different due to local versus global changes in CBF. This is not such an issue for hyperoxic calibration, as Eq. 9.18 is only weakly sensitive to the value of $\alpha$ as changes in CBF are small to negligible. It has been suggested that differences in the measured value of $M$ between hypercapnic and hyperoxic calibration can be accounted for by appropriate selection of $\alpha$ (Mark et al. 2011). Rather than the traditional $\alpha = 0.38$, reflecting total CBV, using a venous CBV-specific $\alpha = 0.23$ produces comparable values of $M$.

In summary, the degree of venous volume change associated with the CBF change is an important question, and further experiments are needed.

## *Is the Davis Model an Accurate Description of the BOLD Effect?*

Many additional simplifying assumptions were made in the derivation of the Davis model. The relationship between $\Delta R_2^*$ and deoxyhemoglobin assumes a simple single-compartment model of gray matter that is dependent on field strength and vessel geometry. Specifically, the only effect included was that of deoxyhemoglobin in venous blood altering the transverse relaxation of the surrounding tissue. This model does not account for signal changes produced by the blood itself (Boxerman et al. 1995) nor does it allow for volume exchange effects (Buxton et al. 2004; Obata et al. 2004; Leontiev and Buxton 2007), when blood volume increases at the expense of extravascular tissue volume and the intrinsic signals from the blood and tissue compartments differ. It is also assumed that changes in $R_2^*$ are small such that its exponential relationship to BOLD may be linearized. While changes in $R_2^*$ do tend to be small, combined with the other assumptions, this adds another source of error to calculations of $CMRO_2$.

Despite these simplifying assumptions, the Davis model continues to be used because associated errors appear to be small, underestimating changes in $CMRO_2$ by only 15% (Chen and Pike 2009). This suggests that, rather than model the additional signal contributions explicitly, optimization of the parameters $\alpha$ and $\beta$ may be the only step necessary in making the Davis model more accurate. In order to perform this optimization, a detailed model of the BOLD signal may be used, rather than noisy experimental data that are likely to result in many local minima (Griffeth

and Buxton 2011a). The detailed model is based upon an earlier BOLD signal model that incorporated both intra- and extravascular signal contributions, but only included the volume exchange effect of venous CBV (Obata et al. 2004). The new model is extended to multiple vascular compartments defined as arterial, capillary, and venous. Existing multicomparment BOLD signal models typically neglect the capillary compartment and distribute this blood volume between the arterial and venous compartments (Lin et al. 2008; Donahue et al. 2009; Blockley et al. 2009). In order to simulate the steady-state BOLD signal using this model, values for the underlying vascular and oxygen saturation effects in all three compartments were gathered from the literature. Following current thinking, the exponent of the Grubb equation for the capillary and venous compartments was set as $\alpha_{c,v}=0.23$ (Chen and Pike 2009). The change in arterial CBV was then determined from the remainder of the total CBV change calculated with $\alpha=0.38$. Parameter optimization was performed on $\alpha$ and $\beta$ of the Davis model using nonlinear optimization. It was found that $\alpha=0.16$ and $\beta=0.9$ improve the accuracy of $CMRO_2$ calculations by the Davis model for 3.0 T measurements (Griffeth and Buxton 2011a). This framework allows further improvements to the values of $\alpha$ and $\beta$ to be incorporated as more evidence is gathered on cerebral hemodynamics.

This approach integrates the extensive research on effectors of the BOLD signal; however, it remains limited, in that it is a steady-state model. The primary limit to extending the model to dynamic measurements of $CMRO_2$ is a more accurate representation of changes in CBV during activation. To achieve this, detailed measurements of the dynamics of the blood volume changes that underlie the BOLD response are required. Currently, this is only possible with the VERVE method (Stefanovic and Pike 2005), but corroboration of these data by alternative new methods would also be useful (Blockley et al. 2010). Acquisition of CBV data, alongside CBF and BOLD, will enable dynamic measurements of $CMRO_2$ to be made. Alternatively, a greater knowledge of the dynamics of venous CBV may be used to improve hemodynamic models in order to avoid acquiring these data in every experiment. With this improved knowledge, our ability to interpret the BOLD response will be greatly improved and will grant us a big step forward in measuring neural activity using MRI.

## Current Studies and Future Directions

Current progress in quantifying the BOLD signal underlines the importance of acquiring complementary data using multiple modalities. In particular, simultaneous measurements of CBF enables variations in physiological baseline to inform the conclusions that can be drawn from BOLD measurements (Brown et al. 2003; Fleisher et al. 2009). The calibrated BOLD method has been used to assess $CMRO_2$ changes to basic stimuli in a number of brain regions (Kastrup et al. 2002; Stefanovic et al. 2004; Chiarelli et al. 2007a; Ances et al. 2008; Leontiev et al. 2007; Leontiev and Buxton 2007) and to explore the physiological response to an

administered drug (St Lawrence et al. 2003; Uludağ and Buxton 2004; Perthen et al. 2008). Direct measurements of venous CBV (Stefanovic and Pike 2005; Blockley et al. 2010) and incorporation of these data into a model of the BOLD response (Lin et al. 2008; Donahue et al. 2009) could enable measurements of dynamic changes in $CMRO_2$. Changes in physiological baseline are common in neuroimaging and can have a diverse range of origins, including the effects of pharmacological manipulations (Brown et al. 2003), disease (Fleisher et al. 2009), neural activity manipulations (Uludağ et al. 2004), or subject attention (Moradi and Buxton 2011). Measurement of steady-state, or slowly changing $CMRO_2$ levels by techniques such as the qBOLD method have particular application in clinical studies where the greater availability of MRI over oxygen-15-based PET is a real advantage (He and Yablonskiy 2007). Similarly, whole-brain measures of $CMRO_2$ (Xu et al. 2009; Jain et al. 2010) provide a good way of assessing the systemic effects caused by conditions such as hypercapnia, hypoxia, or even normal aging (Ances et al. 2009).

## References

An H, Lin W (2000) Quantitative measurements of cerebral blood oxygen saturation using magnetic resonance imaging. J Cereb Blood Flow Metab 20:1225–1236

An H, Lin W (2003) Impact of intravascular signal on quantitative measures of cerebral oxygen extraction and blood volume under normo- and hypercapnic conditions using an asymmetric spin echo approach. Magn Reson Med 50:708–716

Ances BM, Leontiev O, Perthen JE, Liang C, Lansing AE, Buxton RB (2008) Regional differences in the coupling of cerebral blood flow and oxygen metabolism changes in response to activation: implications for BOLD-fMRI. Neuroimage 39:1510–1521

Ances BM, Liang CL, Leontiev O, Perthen JE, Fleisher AS, Lansing AE, Buxton RB (2009) Effects of aging on cerebral blood flow, oxygen metabolism, and blood oxygenation level dependent responses to visual stimulation. Hum Brain Mapp 30:1120–1132

Belliveau JW, Kennedy D, McKinstry R, Buchbinder B, Weisskoff R, Cohen M, Vevea J, Brady T, Rosen B (1991) Functional mapping of the human visual cortex by magnetic resonance imaging. Science 254:716–719

Blockley NP, Francis ST, Gowland PA (2009) Perturbation of the BOLD response by a contrast agent and interpretation through a modified balloon model. Neuroimage 48:84–93

Blockley NP, Driver ID, Fisher JA, Francis ST, Gowland PA (2011) Measuring venous blood volume changes during activation using hyperoxia. Magn Reson Med 59:3266–3274

Bolar DS, Rosen BR, Sorensen AG, Adalsteinsson E (2011) QUantitative Imaging of eXtraction of oxygen and TIssue consumption (QUIXOTIC) using venular-targeted velocity-selective spin labeling. Magn Reson Med 66:1550–1562

Bolar D, Sorensen A, Rosen B, Adalsteinsson E (2009) Feasibility of QUantitative Imaging of eXtraction and TIssue Consumption (QUIXOTIC) to assess functional changes in venous oxygen saturation during visual stimulus. Proceeding ISMRM 17th annual meeting, Honolulu, p 3658

Boxerman JL, Hamberg LM, Rosen BR, Weisskoff RM (1995) MR contrast due to intravascular magnetic susceptibility perturbations. Magn Reson Med 34:555–566

Bremmer JP, van Berckel BNM, Persoon S, Kappelle LJ, Lammertsma AA, Kloet R, Luurtsema G, Rijbroek A, Klijn CJM, Boellaard R (2010). Day-to-day test-retest variability of CBF, CMRO(2), and OEF measurements using dynamic (15)O PET studies. Mol Imaging Biol 13(4):759–768

Brittain JH, Hu BS, Wright GA, Meyer CH, Macovski A, Nishimura DG (1995) Coronary angiography with magnetization-prepared T2 contrast. Magn Reson Med 33:689–696

Brown GG, Eyler Zorrilla LT, Georgy B, Kindermann SS, Wong EC, Buxton RB (2003) BOLD and perfusion response to finger-thumb apposition after acetazolamide administration: differential relationship to global perfusion. J Cereb Blood Flow Metab 23:829–837

Bulte DP, Chiarelli PA, Wise RG, Jezzard P (2007) Cerebral perfusion response to hyperoxia. J Cereb Blood Flow Metab 27:69–75

Buxton RB (2010) Interpreting oxygenation-based neuroimaging signals: the importance and the challenge of understanding brain oxygen metabolism. Front Neuroenerg 2:8

Buxton RB, Wong EC, Frank LR (1998) Dynamics of blood flow and oxygenation changes during brain activation: the balloon model. Magn Reson Med 39:855–864

Buxton R, Uludağ K, Dubowitz D, Liu T (2004) Modeling the hemodynamic response to brain activation. Neuroimage 23:S220–S233

Chen Y, Parrish TB (2009) Caffeine's effects on cerebrovascular reactivity and coupling between cerebral blood flow and oxygen metabolism. Neuroimage 44:647–652

Chen JJ, Pike GB (2009) BOLD-specific cerebral blood volume and blood flow changes during neuronal activation in humans. NMR in Biomed 22:1054–1062

Chen JJ, Pike GB (2010) MRI measurement of the BOLD-specific flow-volume relationship during hypercapnia and hypocapnia in humans. NeuroImage 53:383–391

Chiarelli PA, Bulte DP, Gallichan D, Piechnik SK, Wise R, Jezzard P (2007a) Flow-metabolism coupling in human visual, motor, and supplementary motor areas assessed by magnetic resonance imaging. Magn Reson Med 57:538–547

Chiarelli PA, Bulte DP, Wise R, Gallichan D, Jezzard P (2007b) A calibration method for quantitative BOLD fMRI based on hyperoxia. Neuroimage 37:808–820

Dai W, Garcia D, de Bazelaire C, Alsop DC (2008) Continuous flow-driven inversion for arterial spin labeling using pulsed radio frequency and gradient fields. Magn Reson Med 60:1488–1497

Davis TL, Kwong KK, Weisskoff RM, Rosen BR (1998) Calibrated functional MRI: mapping the dynamics of oxidative metabolism. Proc Natl Acad Sci U S A 95:1834–1839

Derdeyn CP, Videen TO, Yundt KD, Fritsch SM, Carpenter DA, Grubb RL, Powers WJ (2002) Variability of cerebral blood volume and oxygen extraction: stages of cerebral haemodynamic impairment revisited. Brain 125:595–607

Detre JA, Leigh JS, Williams DS, Koretsky AP (1992) Perfusion imaging. Magn Reson Med 23:37–45

Donahue MJ, Lu H, Jones CK, Edden RAE, Pekar JJ, van Zijl PCM (2006) Theoretical and experimental investigation of the VASO contrast mechanism. Magn Reson Med 56:1261–1273

Donahue MJ, Blicher JU, Østergaard L, Feinberg DA, MacIntosh BJ, Miller KL, Günther M, Jezzard P (2009) Cerebral blood flow, blood volume, and oxygen metabolism dynamics in human visual and motor cortex as measured by whole-brain multi-modal magnetic resonance imaging. J Cereb Blood Flow Metab 29:1856–1866

Fleisher AS PodrazaKM, Bangen KJ, Taylor C, Sherzai A, Sidhar K, Liu TT, Dale AM, Buxton RB (2009) Cerebral perfusion and oxygenation differences in Alzheimer's disease risk. Neurobiol Aging 30:1737–1748

Fox PT, Raichle ME (1986) Focal physiological uncoupling of cerebral blood flow and oxidative metabolism during somatosensory stimulation in human subjects. Proc Natl Acad Sci U S A 83:1140–1144

Francis ST, Bowtell R, Gowland PA (2008) Modeling and optimization of Look-Locker spin labeling for measuring perfusion and transit time changes in activation studies taking into account arterial blood volume. Magn Reson Med 59:316–325

Gauthier C, Madjar C, Tancredi F, Stefanovic B, Hoge R (2011) Elimination of visually evoked BOLD responses during carbogen inhalation: Implications for calibrated MRI. NeuroImage 54:1001–1011

Griffeth VEM, Buxton RB (2011a) A theoretical framework for estimating cerebral oxygen metabolism changes using the calibrated-BOLD method: Modeling the effects of blood volume distribution, hematocrit, oxygen extraction fraction, and tissue signal properties on the BOLD signal. NeuroImage 58:198–212

Griffeth VEM, Perthen JE, Buxton RB (2011b) Prospects for quantitative fMRI: Investigating the effects of caffeine on baseline oxygen metabolism and the response to a visual stimulus in humans. NeuroImage 57:809–816

Grubb RL, Raichle ME, EichLing JO, Ter-Pogossian MM (1974) The effects of changes in PaCO2 cerebral blood volume, blood flow, and vascular mean transit time. Stroke 5:630–639

Guo J, Wong EC (2012) Venous oxygenation mapping using velocity-selectiveexcitation and arterial nulling. Magn Reson Med 68:1458–1471

Guyton AC (1991) Textbook of medical physiology, 8th edn. W. B. Saunders, Philadelphia

He X, Yablonskiy DA (2007) Quantitative BOLD: mapping of human cerebral deoxygenated blood volume and oxygen extraction fraction: default state. Magn Reson Med 57:115–126

Herman P, Sanganahalli BG, Blumenfeld H, Hyder F (2009) Cerebral oxygen demand for short-lived and steady-state events. J Neurochem 109(Suppl 1):73–79

Hillman EMC, Devor A, Bouchard MB, Dunn AK, Krauss GW, Skoch J, Bacskai BJ, Dale AM, Boas DA (2007) Depth-resolved optical imaging and microscopy of vascular compartment dynamics during somatosensory stimulation. Neuroimage 35:89–104

Hoge RD, Atkinson J, Gill B, Crelier GR, Marrett S, Pike GB (1999) Investigation of BOLD signal dependence on cerebral blood flow and oxygen consumption: the deoxyhemoglobin dilution model. Magn Reson Med 42:849–863

Jain V, Langham MC, Wehrli FW (2010) MRI estimation of global brain oxygen consumption rate. J Cereb Blood Flow Metab 30:1598–1607

Kastrup A, Krüger G, Neumann-Haefelin T, Glover GH, Moseley ME (2002) Changes of cerebral blood flow, oxygenation, and oxidative metabolism during graded motor activation. Neuroimage 15:74–82

Kida I, Rothman D, Hyder F (2007) Dynamics of changes in blood flow, volume, and oxygenation: implications for dynamic functional magnetic resonance imaging calibration. J Cereb Blood Flow Metab 27:690–696

Kim T, Kim S (2006) Quantification of cerebral arterial blood volume using arterial spin labeling with intravoxel incoherent motion-sensitive gradients. Magn Reson Med 55:1047–1057

Kim SG, Rostrup E, Larsson HB, Ogawa S, Paulson OB (1999) Determination of relative CMRO2 from CBF and BOLD changes: significant increase of oxygen consumption rate during visual stimulation. Magn Reson Med 41:1152–1161

Kim T, Hendrich K, Masamoto K, Kim S (2007) Arterial versus total blood volume changes during neural activity-induced cerebral blood flow change: implication for BOLD fMRI. J Cereb Blood Flow Metab 27:1235–1247

Lammertsma AA (1984) Positron emission tomography of the brain: measurement of regional cerebral function in man. Clin Neurol Neurosurg 86:1–11

Lee S, Duong T, Yang G, Iadecola C, Kim S (2001) Relative changes of cerebral arterial and venous blood volumes during increased cerebral blood flow: implications for BOLD fMRI. Magn Reson Med 45:791–800

Leontiev O, Buxton RB (2007) Reproducibility of BOLD, perfusion, and CMRO2 measurements with calibrated-BOLD fMRI. Neuroimage 35:175–184

Leontiev O, Dubowitz DJ, Buxton RB (2007) CBF/CMRO2 coupling measured with calibrated BOLD fMRI: sources of bias. Neuroimage 36:1110–1122

Lin A, Fox PT, Yang Y, Lu H, Tan L, Gao J (2008) Evaluation of MRI models in the measurement of CMRO2 and its relationship with CBF. Magn Reson Med 60:380–389

Lu H, Ge Y (2008) Quantitative evaluation of oxygenation in venous vessels using T2-Relaxation-Under-Spin-Tagging MRI. Magn Reson Med 60:357–363

Lu H, Golay X, Pekar JJ, Zijl PCV (2003) Functional magnetic resonance imaging based on changes in vascular space occupancy. Magn Reson Med 50:263–274

Marchal G, Rioux P, Petit-Taboué MC, Sette G, Travère JM, Le Poec C, Courtheoux P, Derlon JM, Baron JC (1992) Regional cerebral oxygen consumption, blood flow, and blood volume in healthy human aging. Arch Neurol 49:1013–1020

Mark CI, Fisher JA, Pike GB (2011) Improved fMRI calibration: precisely controlled hyperoxic versus hypercapnic stimuli. Neuroimage 54:1102–1111

Mintun MA, Raichle ME, Martin WRW, Herscovitch P (1984) Brain oxygen utilization measured with O-15 radiotracers and positron emission tomography. J Nucl Med 25:177–187
Moradi F, Buračas GT, Buxton RB (2012) Attention strongly increases oxygen metabolic response to stimulus in primary visual cortex. Neuroimage 59(1):601–607
Obata T, Liu TT, Miller KL, Luh WM, Wong EC, Frank LR, Buxton RB (2004) Discrepancies between BOLD and flow dynamics in primary and supplementary motor areas: application of the balloon model to the interpretation of BOLD transients. Neuroimage 21:144–153
Ogawa S, Lee TM, Kay AR, Tank DW (1990) Brain magnetic resonance imaging with contrast dependent on blood oxygenation. Proc Natl Acad Sci U S A 87:9868–9872
Ogawa S, Menon RS, Tank DW, Kim SG, Merkle H, Ellermann JM, Uğurbil K (1993) Functional brain mapping by blood oxygenation level-dependent contrast magnetic resonance imaging. A comparison of signal characteristics with a biophysical model. Biophys J 64:803–812
Pauling L, Coryell CD (1936) The magnetic properties and structure of the hemochromogens and related substances. Proc Natl Acad Sci U S A 22:159–163
Pears JA, Francis ST, Butterworth SE, Bowtell RW, Gowland PA (2003) Investigating the BOLD effect during infusion of Gd-DTPA using rapid T2* mapping. Magn Reson Med 49:61–70
Perthen JE, Lansing AE, Liau J, Liu TT, Buxton RB (2008) Caffeine-induced uncoupling of cerebral blood flow and oxygen metabolism: a calibrated BOLD fMRI study. Neuroimage 40:237–247
Petersen ET, Lim T, Golay X (2006) Model-free arterial spin labeling quantification approach for perfusion MRI. Magn Reson Med 55:219–232
Prisman E, Slessarev M, Han J, Poublanc J, Mardimae A, Crawley A, Fisher J, Mikulis D (2008) Comparison of the effects of independently-controlled end-tidal PCO2 and PO2 on blood oxygen level-dependent BOLD MRI. J Magn Reson Imag 27:185–191
Rostrup E, Knudsen GM, Law I, Holm S, Larsson HBW, Paulson OB (2005) The relationship between cerebral blood flow and volume in humans. Neuroimage 24:1–11
Severinghaus JW (1979) Simple, accurate equations for human blood O2 dissociation computations. J Appl Physiol 46:599–602
Sicard K, Duong T (2005) Effects of hypoxia, hyperoxia, and hypercapnia on baseline and stimulus-evoked BOLD, CBF, and CMRO2 in spontaneously breathing animals. Neuroimage 25:850–858
Silvennoinen MJ, Clingman CS, Golay X, Kauppinen RA, van Zijl PCM (2003) Comparison of the dependence of blood R2 and R2* on oxygen saturation at 1.5 and 4.7 Tesla. Magn Reson Med 49:47–60
Spees WM, Yablonskiy DA, Oswood MC, Ackerman JJ (2001) Water proton MR properties of human blood at 1.5 Tesla: magnetic susceptibility, T1, T2, T2*, and non-Lorentzian signal behavior. Magn Reson Med 45:533–42
Stefanovic B, Pike GB (2005) Venous refocusing for volume estimation: VERVE functional magnetic resonance imaging. Magn Reson Med 53:339–347
Stefanovic B, Warnking JM, Pike GB (2004) Hemodynamic and metabolic responses to neuronal inhibition. Neuroimage 22:771–778
St Lawrence KS, Ye FQ, Lewis BK, Frank JA, McLaughlin AC (2003) Measuring the effects of indomethacin on changes in cerebral oxidative metabolism and cerebral blood flow during sensorimotor activation. Magn Reson Med 50:99–106
Thulborn KR, Waterton JC, Matthews PM, Radda GK (1982) Oxygenation dependence of the transverse relaxation time of water protons in whole blood at high field. Biochim Biophys Acta 714:265–270
Uludağ K (2010) To dip or not to dip: reconciling optical imaging and fMRI data. Proc Natl Acad Sci U S A 107:E23 (author reply E24)
Uludağ K, Buxton RB (2004) Measuring the effects of indomethacin on changes in cerebral oxidative metabolism and cerebral blood flow during sensorimotor activation. Magn Reson Med 51:1088–1089 (author reply 1090)
Uludağ K, Dubowitz DJ, Yoder EJ, Restom K, Liu TT, Buxton RB (2004) Coupling of cerebral blood flow and oxygen consumption during physiological activation and deactivation measured with fMRI. Neuroimage 23:148–155

Uludağ K, Müller-Bierl B, Uğurbil K (2009) An integrative model for neuronal activity-induced signal changes for gradient and spin echo functional imaging. Neuroimage 48:150–165

Vafaee MS, Gjedde A (2000) Model of blood-brain transfer of oxygen explains nonlinear flow-metabolism coupling during stimulation of visual cortex. J Cereb Blood Flow Metab 20:747–754

Vafaee MS, Meyer E, Marrett S, Paus T, Evans AC, Gjedde A (1999) Frequency-dependent changes in cerebral metabolic rate of oxygen during activation of human visual cortex. J Cereb Blood Flow Metab 19:272–277

Villringer A, Rosen BR, Belliveau JW, Ackerman JL, Lauffer RB, Buxton RB, Chao YS, Wedeen VJ, Brady TJ (1988) Dynamic imaging with lanthanide chelates in normal brain: contrast due to magnetic susceptibility effects. Magn Reson Med 6:164–174

Vorstrup S, Henriksen L, Paulson OB (1984) Effect of acetazolamide on cerebral blood flow and cerebral metabolic rate for oxygen. J Clin Invest 74:1634–1639

Wise RG, Pattinson KTS, Bulte DP, Chiarelli PA, Mayhew SD, Balanos GM, O'Connor DF, Pragnell TR, Robbins PA, Tracey I, Jezzard P (2007) Dynamic forcing of end-tidal carbon dioxide and oxygen applied to functional magnetic resonance imaging. J Cereb Blood Flow Metab 27:1521–1532

Wong EC, Buxton RB, Frank LR (1997) Implementation of quantitative perfusion imaging techniques for functional brain mapping using pulsed arterial spin labeling. NMR in Biomed 10:237–249

Xu F, Ge Y, Lu H (2009) Noninvasive quantification of whole-brain cerebral metabolic rate of oxygen (CMRO2) by MRI. Magn Reson Med 62:141–148

Xu F, Yezhuvath U, Wang P, Lu H (2010a) Hypoxia and hyperoxia alter brain metabolism in awake human. Proceeding ISMRM 18th annual meeting, Stockholm, p 1137

Xu F, Uh J, Brier MR, Hart J, Yezhuvath US, Gu H, Yang Y, Lu H (2010b) The influence of carbon dioxide on brain activity and metabolism in conscious humans. J Cereb Blood Flow Metab 31:58–67

Yablonskiy DA (1998) Quantitation of intrinsic magnetic susceptibility-related effects in a tissue matrix. Phantom study. Magn Reson Med 39:417–428

Yablonskiy DA, Haacke EM (1994) Theory of NMR signal behavior in magnetically inhomogeneous tissues: the static dephasing regime. Magn Reson Med 32:749–63

Zappe A, Uludağ K, Oeltermann A, Uğurbil K, Logothetis N (2008) The influence of moderate hypercapnia on neural activity in the anesthetized nonhuman primate. Cereb Cortex 18: 2666–2673